WATER RESOURCES RESEARCH, VOL. 32, NO. 1, PAGES 9–22, JANUARY 1996

64608

Vapor transport of trichloroethylene in the unsaturated zone: Field and numerical modeling investigations

Bernadette Hughes Conant, Robert W. Gillham, and Carl A. Mendoza[1]
Waterloo Centre for Groundwater Research, University of Waterloo, Waterloo, Ontario, Canada

Abstract. Vapor transport of chlorinated solvents in the unsaturated zone may be an important mechanism for the spread of contamination at spill sites and may be a significant factor controlling the extent of groundwater contamination. Two field experiments were carried out at the Canadian Forces Base Borden field site to provide detailed monitoring of the transport behavior of trichloroethylene vapors in the unsaturated zone. Experiments were conducted for both winter and summer conditions and under different surface boundary conditions. The observed results were simulated using a Fickian-based numerical model with linear equilibrium phase partitioning. The model includes both diffusion and density-induced advection and allows for the incorporation of spatial heterogeneities and nonisothermal conditions. Numerical sensitivity analyses were conducted to further evaluate the relative influence of various transport parameters on vapor migration. Use of measured field values as input parameters resulted in a very good match between the experimental results and numerical simulations. In both experiments, vapor plumes spread several meters from the source and downward to the capillary fringe within only a few days. Seasonal temperature variations were found to have a significant impact on the rate and total mass of vapor transport, and variations in organic carbon content, and to a lesser extent moisture content, exerted the greatest control on retardation of vapor migration. Transport was diffusion dominated, but density-induced advection was an appreciable component of net transport under summer conditions, when vapor concentrations were higher. Geologic conditions at the site made overall transport relatively insensitive to the ground surface boundary condition.

Introduction

Trichloroethylene (TCE) and other chlorinated organic solvents (hereinafter referred to as solvents) are among the most frequently identified contaminants in groundwater. Within the last decade, researchers have investigated various aspects of the subsurface migration of solvents and other dense nonaqueous phase liquids (DNAPL) that contribute to a vast array of complex groundwater remediation problems. Most of this research has focused on physical and chemical processes relevant to migration within the saturated zone. However, because solvents are volatile, the air-filled porosity of the unsaturated zone also provides a pathway for contaminant migration. The potential for solvent vapor transport to contribute significantly to contamination of underlying groundwater was recognized by *Schwille* [1984, 1988], and has been investigated through computer simulations [*Sleep and Sykes*, 1989; *Mendoza and McAlary*, 1990].

As a solvent liquid migrates downward through the unsaturated zone following a spill, some of it will become trapped in the pore spaces at residual saturation. Volatilization of this residual solvent will result in the formation of a vapor phase contaminant plume within the soil gas. The plume will spread by vapor diffusion and, potentially, by density-induced advection of the soil gas mixture [*Falta et al.*, 1989; *Mendoza and Frind*, 1990a]. As it spreads, the vapor plume will also cause contamination of the soil moisture and soil matrix as a result of phase partitioning. Contamination of the underlying groundwater can ultimately occur by way of vapor migration downward to the capillary fringe, a rise of the water table into the contaminated zone, or infiltration of groundwater recharge through contaminated areas. Thus the potential exists for vapor plumes to contaminate large areas of shallow groundwater over relatively short time frames. As a first step in an investigation of this phenomenon, a better understanding of the primary processes controlling solvent vapor transport in the unsaturated zone is required.

The purpose of this study is to provide a detailed, field-scale analysis of the transport behavior of solvent vapors within the unsaturated zone. The study was conducted at Canadian Forces Base Borden in Ontario, and included two experiments designed to map the spread of TCE vapors from a source of residual TCE liquid in the sandy unsaturated deposits. The first experiment (experiment 1) examined vapor transport during the winter under conditions of a covered ground surface. A second, similar experiment, conducted the following summer (experiment 2), examined transport for an uncovered ground surface. The results of the experiments were compared to numerical simulations incorporating both diffusion and density-induced flow processes, equilibrium phase partitioning, and the effects of spatial heterogeneities and nonisothermal conditions. The significance of spatial variations in site characteristics was also considered. Additional sensitivity analyses were

[1]Now at Department of Earth and Atmospheric Sciences, University of Alberta, Edmonton, Canada.

Copyright 1996 by the American Geophysical Union.

Paper number 95WR02965.
0043-1397/96/95WR-02965$05.00

11585

performed using the numerical model to gain insight into the relative importance of various factors on vapor transport.

Theoretical Background

For the transport scenarios examined in this study, the primary mechanisms of interest are diffusion of contaminant vapors within the porous matrix, and advective flow of the soil gas mixture. The applicable advection-dispersion equation for transport of a single reactive component in the vapor phase, expressed in axisymmetric coordinates, is

$$\frac{1}{r}\frac{\partial}{\partial x_i}\left[r\theta_g D_{ij}\frac{\partial C_g}{\partial x_j}\right] - \nu_i\frac{\partial}{\partial x_i}[\theta_g C_g] = \theta_g R\frac{\partial C_g}{\partial t} \qquad (1)$$

$$i, j = r, z$$

where θ_g is the gas-filled porosity $[L^3\ L^{-3}]$, D_{ij} is the dispersion tensor $[L^2\ T^{-1}]$, as described by *Bear* [1972], C_g is the contaminant concentration in the soil gas [mol L^{-3}], ν is the average linear advective velocity of the gas mixture $[L\ T^{-1}]$, and R is the retardation factor (dimensionless). The dispersion coefficient D can be expanded further as

$$D = \alpha\nu + \tau D_a \qquad (2)$$

where α is the dispersivity of the porous medium $[L]$, D_a is the free-air diffusion coefficient $[L^2\ T^{-1}]$, and τ is the tortuosity. If the advective flow velocities are large, then advective transport may be important, or even dominant, relative to diffusion. Conversely, if the velocities are very small, then the second term in (1) becomes negligible, the dispersion coefficient D becomes an effective diffusion coefficient, and the transport equation reduces to Fick's second law of diffusion modified for a reactive constituent.

Free-air diffusion coefficients for organic compounds are several orders of magnitude larger than aqueous diffusion coefficients. As a result, diffusion is generally more significant for contaminant transport in soil gas than in groundwater, and calculation of diffusive fluxes is a more critical component of transport predictions. The validity of the assumptions inherent in diffusion-based equations for vapor transport has recently been examined by several researchers [*Thorstenson and Pollock*, 1989; *Baehr and Bruell*, 1990; *Abriola et al.*, 1992; *Massmann and Farrier*, 1992]. Studies such as those by *Abriola et al.* [1992] and *Massmann and Farrier* [1992] suggest that formulations such as (1) are suitable for describing vapor transport in relatively coarse grained sediments, like those considered in this study.

Rates of vapor diffusion within the unsaturated zone will be affected by variations in both moisture content and temperature. As moisture contents increase near the capillary fringe or in finer-grained layers, the cross-sectional area of the pore space available for vapor diffusion is reduced, and the diffusion pathways become more convoluted. These effects are accounted for in the dispersion coefficient (2) through use of an empirical relationship [*Millington and Quirk*, 1961] to calculate the tortuosity factor. The effect of variable temperatures on vapor diffusion rates is reflected in the temperature dependence of the free-air diffusion coefficient. However, unsaturated zone temperature variations typically encountered in most climates will have only a small effect on diffusion rates. For example, a temperature increase of 10°C, from 10°C to 20°C, corresponds to an increase in the free-air diffusion coefficient for TCE of just over 6% [*Mendoza and Frind*, 1990b].

Advective transport of vapors due to flow of the soil gas mixture is described by the second term on the left-hand side of (1). For volatile compounds of relatively high molecular weight, such as chlorinated solvents, significant concentration-dependent density gradients can develop in the vicinity of the organic liquid. The potential for these density gradients to result in advective flow of soil gas has been demonstrated numerically [*Falta et al.*, 1989; *Mendoza and Frind*, 1990a].

In addition to advection induced by density gradients, soil gas flow can also occur as a result of pressure gradients caused by barometric pressure fluctuations [*Massmann and Farrier*, 1992], vaporization of a liquid [*Baehr and Bruell*, 1990; *Mendoza and Frind*, 1990b], or water table fluctuations [*Weeks et al.*, 1982]. Over the course of this study, atmospheric pressure variations were small, with a maximum measured change of 10 mbar over 24 hours for experiment 2. Therefore for the experimental conditions in this study, advection due to barometric pressure changes was assumed to be negligible [*Massmann and Farrier*, 1992]. As was discussed by *Mendoza and Frind* [1990b], the contribution of liquid vaporization to pressure gradients is not likely to be significant in situations such as those examined in this study because the vapor pressure of TCE is not sufficiently high. Advective effects due to water table fluctuations, which were of the order of 0.1 to 0.4 m, were also assumed negligible. Thus for this study, density gradients are the only cause of advective transport considered in the numerical analysis.

The advective flow of soil gas in response to density gradients can be generally described by equations similar to the used for density flow of groundwater during saltwater intrusion. Inherent in the soil gas formulation are the assumptions that flow is laminar, that the soil gas behaves as an incompressible phase with respect to flow, and that gas slippage along pore walls is negligible. These assumptions are expected to be reasonable for the passive transport scenario, sandy geology, and small pressure gradients encountered in the Borden experiments [*Massmann*, 1989; *McWhorter*, 1990]. The flow equation used in this study, expressed in axisymmetric coordinates, is of the form [*Mendoza and Frind*, 1990a]

$$\frac{1}{r}\frac{\partial}{\partial x_i}\left[rk_r k_{ij}\frac{\rho_0 g}{\mu}\rho\left(\frac{\partial h^*}{\partial x_j} + \frac{\rho - \rho_0}{\rho_0}\right)\frac{\partial z}{\partial x_j}\right]$$

$$= \theta_g\rho_0 g\frac{\rho}{P}\frac{\partial h^*}{\partial t} \qquad i, j = r, z \qquad (3)$$

where k_{ij} is the intrinsic permeability $[L^2\ T^{-1}]$, ρ is the density of the gas mixture $[M\ L^{-3}]$, ρ_0 is the density of uncontaminated soil gas $[M\ L^{-3}]$, g is the gravitational constant $[L\ T^{-2}]$, μ is the viscosity of the gas mixture $[M\ T^{-1}\ L^{-1}]$, and P is the fluid pressure $[M\ T^{-2}\ L^{-1}]$. The equivalent head of the gas mixture (h^*) is defined as $h^* = P/\rho_0 g + z$.

Advective soil gas transport is sensitive to both the magnitude and degree of spatial variability of gas phase permeabilities at the site, which are a function of both the intrinsic permeability and moisture content of the sands. Prior to conducting the study, it was not known whether a significant advective component of TCE vapor transport should be expected. The intrinsic permeability values measured for the site, of the order of 10^{-11} m^2, are close to the values suggested by earlier numerical modeling studies as a probable lower limit for significant density-driven advective flow [*Falta et al.*, 1989;

Mendoza and McAlary, 1990; *Mendoza and Frind*, 1990b]. For the majority of the unsaturated zone profile, which was at or near residual moisture content, soil moisture is expected to reduce gas phase permeabilities only moderately. For these well-drained sands, a gas phase relative permeability (k_r) of 0.8 was assumed. For higher moisture content zones, where a more significant reduction of gas phase permeability is expected, the value for k_r was approximated by the relationship of *Brooks and Corey* [1964], using a pore size distribution index of 2.0.

The soil gas densities contributing to the density-induced flow described in (3) are a function of vapor concentration. Therefore advective transport is sensitive to the vapor pressure of the solvent, which determines the vapor concentration within the area of the liquid source. Vapor pressure is a sensitive function of temperature for most solvents. Figure 1 compares two temperature regression equations for TCE vapor pressure to single values from various literature sources. The subsurface temperature ranges for the Borden vapor transport experiments, as indicated, encompass a fourfold variation in the vapor pressure of TCE. Therefore the temperature variations encountered in these experiments are expected to significantly influence the magnitude of driving forces contributing to any density-induced flow.

Viscosity of the soil gas is also temperature dependent, but viscosity variations are not expected to have a large effect on transport. A temperature increase of 20°C (from 0°C to 20°C), similar to the range of temperatures encountered in this study, results in an increase in the viscosity of uncontaminated air of only 5–6% [*Bird et al.*, 1960].

Partitioning of vapors to the soil moisture and solid matrix affects net vapor transport and determines the distribution of the contaminant mass in the unsaturated zone. The effects on transport of interaction of the vapor plume with the aquifer are incorporated in the right-hand side of (1) as a retardation factor R, which can be expressed in the form [*Weeks et al.*, 1982; *Baehr*, 1987; *Mendoza and Frind*, 1990a]:

$$R = 1 + \frac{\theta_w}{\theta_g}\frac{1}{H} + \frac{\rho_b}{\theta_g H} K_d \qquad (4)$$

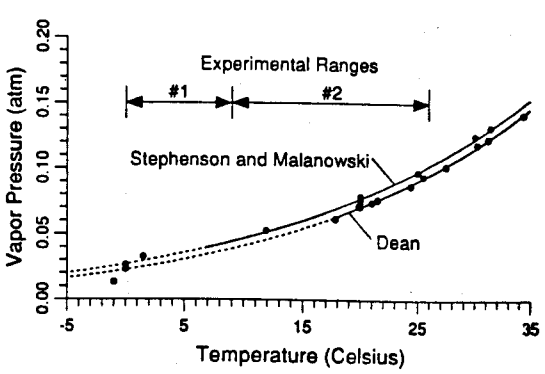

Figure 1. Trichloroethylene (TCE) vapor pressure versus temperature. Individual points represent single-temperature values from literature sources [*Boublik et al.*, 1984; *Cohen and Ryan*, 1985; *Dean*, 1985; *Dilling*, 1977; *Dilling et al.*, 1975; *Flick*, 1985; *Hansch and Leo*, 1979; *Love and Eilers*, 1982; *Mackay and Shiu*, 1981; *Peterson et al.*, 1988; *Schwille*, 1988; *Stephenson and Malanowski*, 1987; *Weast*, 1987].

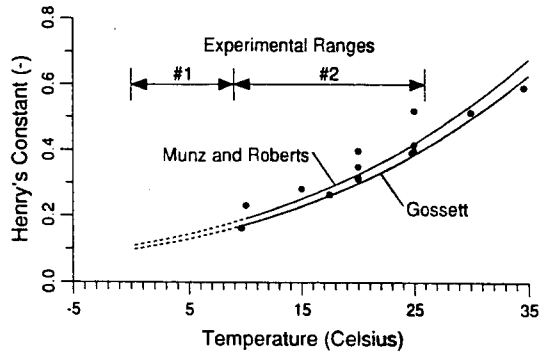

Figure 2. Value of dimensionless form of the Henry's law constant for TCE versus temperature. Individual points represent single-temperature values from literature sources [*Cohen and Ryan*, 1985; *Dilling*, 1987; *Garbarini and Lion*, 1985; *Gossett*, 1987; *Hutzler et al.*, 1989; *Munz and Roberts*, 1987; *Schwille*, 1988; *Thompson and Marrin*, 1987].

where θ_w is the water-filled porosity [$L^3\ L^{-3}$], H is the Henry's constant [mol L^{-3} (mol L^{-3})$^{-1}$], ρ_b is the bulk density of the porous medium [$M\ L^{-3}$], and K_d is the equilibrium solid-aqueous phase partitioning coefficient [$L^3\ M^{-1}$]. This relationship assumes that chemical equilibrium exists between the contaminant in the vapor, dissolved, and sorbed phases and that mass transfer between phases is reversible and not kinetically limited.

Partitioning of the contaminant between the soil gas and soil moisture is governed by Henry's constant H, which is defined for a specific temperature and pressure. Figure 2 compares two temperature regression relationships for H to single measurements taken from literature sources; the temperature dependence of H is significant. Because the range of values shown reflects a threefold increase in the value of H for the study conditions, dissolution of vapors into the soil moisture (and resultant sorption onto the soil solids) is significantly influenced by temperature variations.

The effect of sorption of hydrophobic organic contaminants to the aquifer solids is accounted for by the K_d term in (4). Use of a solid-aqueous phase partitioning coefficient infers that all sorption to the aquifer matrix occurs from the dissolved contamination in the soil moisture and not directly from the vapor phase. Neglecting direct vapor-solid sorption underestimates sorption significantly only at very low moisture contents, below those typically encountered in most soils in humid or temperate climates [*Chiou and Shoup*, 1985; *Peterson et al.*, 1988; *Poe et al.*, 1988; *Smith et al.*, 1990].

The spatial variability in organic carbon content of approximately 2 orders of magnitude at the study site is expected to have a significant effect on the retardation of vapor transport. For the numerical analysis, K_d values were calculated, based on the fraction of organic carbon (f_{oc}) of the soil. This approach has been found to be generally applicable for soils with f_{oc} values greater than 0.001 [*Schwartzenbach and Westall*, 1981; *Karickhoff*, 1984]. However, some of the f_{oc} values measured at the study site fell below this value. For those portions of the site with very low levels of organic carbon, the approximation of K_d based on organic carbon content may underpredict sorption [*Schwartzenbach and Westall*, 1981; *Piwoni and Banerjee*, 1989; *Larsen et al.*, 1989; *Curtis et al.*, 1986].

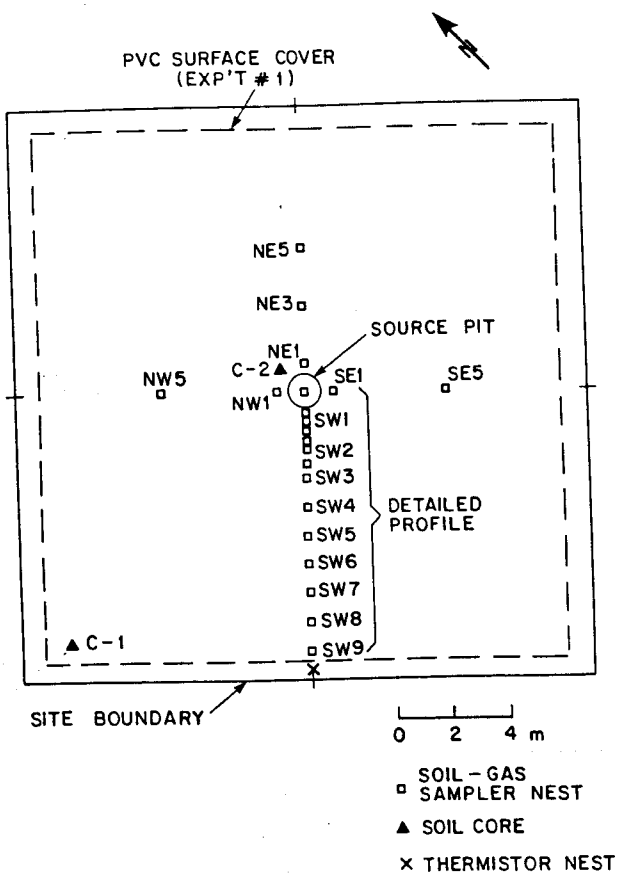

Figure 3. Plan view of experimental site and layout of instrumentation. Nomenclature of soil gas sampler nests reflects compass direction (e.g., NW) and distance in meters (e.g., NW5) from source.

Field Experiments

Experimental Setup

The vapor transport experiments were conducted in the unsaturated zone at Canadian Forces Base Borden, Ontario, approximately 100 m north of the location of previous Borden saturated-zone studies [*Sudicky*, 1986; *Mackay et al.*, 1986]. The two experiments were conducted over the same 20 m × 20 m area (Figure 3). Experiment 1 was conducted in the winter (November–December); the surface of the site was covered with a sheet of 0.5-mm-thick (20 mil) polyvinyl chloride (PVC) plastic to reduce both vapor loss to the atmosphere and infiltration of precipitation to the unsaturated zone. Experiment 2 was conducted during the following summer (July–August) with the ground surface uncovered, except for a very small circular cover (0.8-m radius) in the center of the site to prevent infiltration directly through the TCE source.

A source of TCE vapors was established for each experiment by burying a mixture of sand and liquid TCE in the shallow subsurface. Sand was excavated from the site and mixed with laboratory grade liquid TCE in a mortar mixer at approximately 4% TCE by volume, which, based on site-specific testing, was found to be an appropriate ratio to establish a residual (immobile) source. The mixture was then packed into the original excavation. The source zone was cylindrical with a vertical axis of 0.8 m and a diameter of 1.2 m, and the top of the source zone was located 0.35 m below ground surface. Use of a source with a well-defined geometry and a relatively homogeneous distribution of liquid TCE was chosen for ease of comparison to the numerical model.

Site Description

The unsaturated zone at the site is approximately 3.5 m thick and comprises the upper portion of the sequence of glaciolacustrine sands and silts of the Borden aquifer. A schematic cross section through the site is shown in Figure 4. This section is oriented northeast-southwest along the detailed sampling profile indicated in Figure 3. The section is divided into a lower and an upper section of sands by a thin (3–10 cm) layer of organic-rich, silty, fine sand ("organic horizon") which is laterally continuous over the southern two thirds of the site. The lower section of the unsaturated zone is composed of laminated sands overlain by a more massive (unlaminated) unit which grades upward to the organic horizon. Deposits overlying the organic horizon consist of heterogeneous sands and discontinuous layers of dark brown, organic-rich, silty sand.

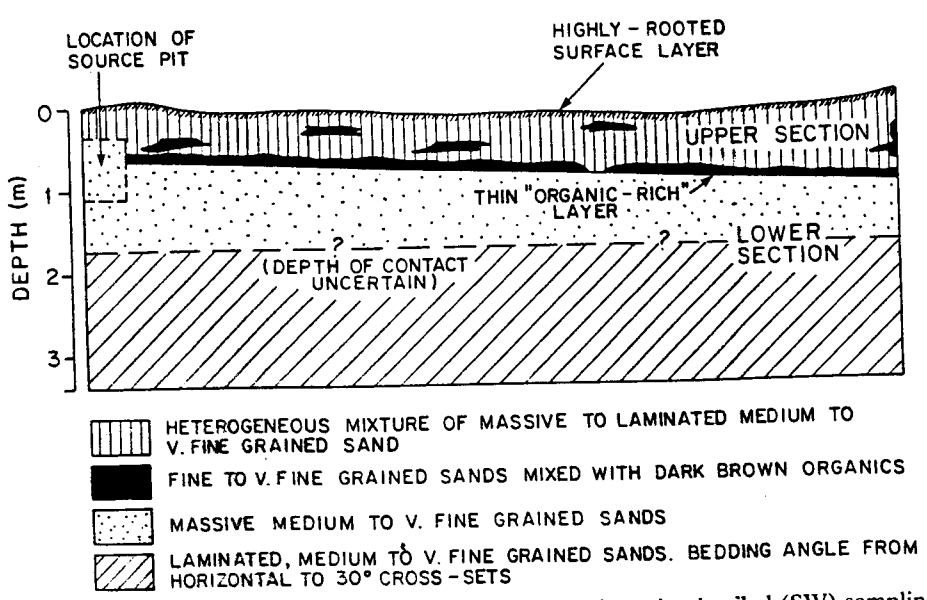

Figure 4. Schematic section of the unsaturated zone sediments along the detailed (SW) sampling profile.

Soil development is minimal and is restricted to a 2- to 10-cm thick layer with abundant roots and accumulated plant debris.

A continuous sediment profile of f_{oc} was created from analyses of soil samples from a core at location C2 (Figure 3). These samples were analyzed using the dry combustion method described by *Churcher and Dickhout* [1987]. As presented in Figure 5a, the highest f_{oc} values, 0.022 and 0.019, correspond to the surficial organic mat and the organic horizon, respectively. Beneath the organic horizon, the f_{oc} declines rapidly with depth, yielding an average value for the lower sands of 0.00021 over 25 samples; a decrease of two orders of magnitude relative to the upper section.

Soil moisture content was determined by gravimetric analysis of sediment samples of known volume collected from locations C1 and C2 (Figure 3) prior to the start of the second experiment. The C1 samples were collected from the center of an area which had been covered with a large section of PVC sheeting for 8 months in order to approximate static drainage conditions. Moisture contents obtained for location C2, where the ground surface was uncovered, were very similar to C1, suggesting that the site was well drained at the start of experiment 2. Moisture contents for the numerical simulations were based on the results for the C2 profile because they were most representative of conditions near the soil gas probes and the source. The volumetric moisture contents for location C2, and the approximated profile used in the simulations, are shown in Figure 5b.

Subsurface temperatures were monitored over the course of the experiments with a nest of seven thermistors installed at 0.5-m depth intervals at the edge of the site (Figure 3). Temperature variations with depth and seasonal variations between winter (experiment 1) and summer (experiment 2), are shown in Figure 6. With the exception of the top few centimeters, the temperature profiles were constant within a few degrees Celsius over the duration of each experiment.

Detailed hydraulic conductivity measurements were performed on two continuous cores obtained immediately adjacent to the study site. The cores were divided into 5-cm subsections, and each was analyzed by a falling-head permeameter test using the method described by *Sudicky* [1986]. Saturated hydraulic conductivity values (for water at 23°C) ranged from 2.8×10^{-5} to 2.4×10^{-4} m s^{-1} with an average of 1.3×10^{-4} m s^{-1} over 167 samples. After the elevations of core segments were adjusted to account for stratigraphic dips and core losses,

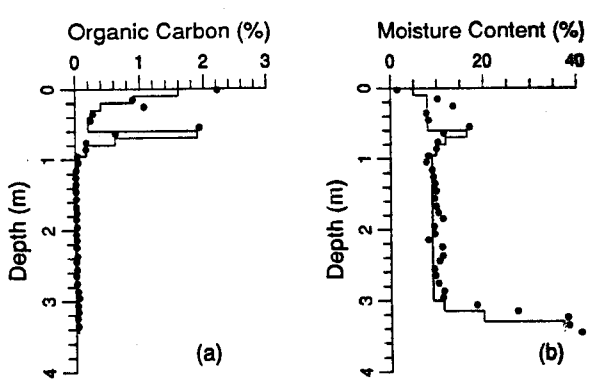

Figure 5. Variations with depth of (a) organic carbon content, and (b) volumetric moisture content. Solid circles represent measured field values; solid lines represent the approximations used in the numerical simulations.

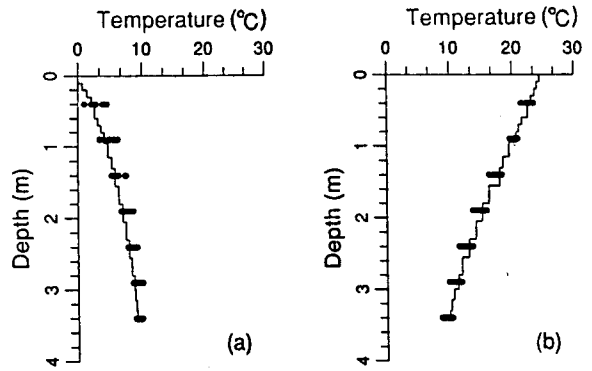

Figure 6. Variation with depth of temperature for (a) experiment 1 (winter) and (b) experiment 2 (summer). Solid circles represent measured field values; solid lines represent the approximations used in the numerical simulations.

hydraulic conductivity values were averaged and converted to intrinsic permeability values [*Freeze and Cherry*, 1979] to provide depth-dependent values for the numerical simulations. Figure 7 compares the depth-corrected permeability values from a core located near the southwest end of the detailed sampling profile to the averaged depth profile used in the model.

Estimates of the total porosity were based on the dry sediment weights from the moisture content samples and a solids density of 2.71 g cm^{-3} [*Ball et al.*, 1990]. These estimates for the unsaturated samples ranged from 41 to 56%. On the basis of discussions with other researchers who had measured porosity for similar conditions in the Borden unsaturated zone, a uniform porosity of 40% was used for the numerical simulations.

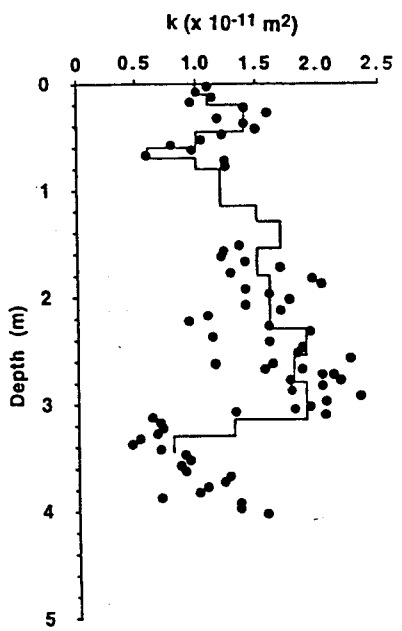

Figure 7. Variation with depth of intrinsic permeability. Solid circles represent measured field values for a core located at the southwest end of the detailed (SW) sampling profile. The solid line represents the averaged profile used in the numerical simulations.

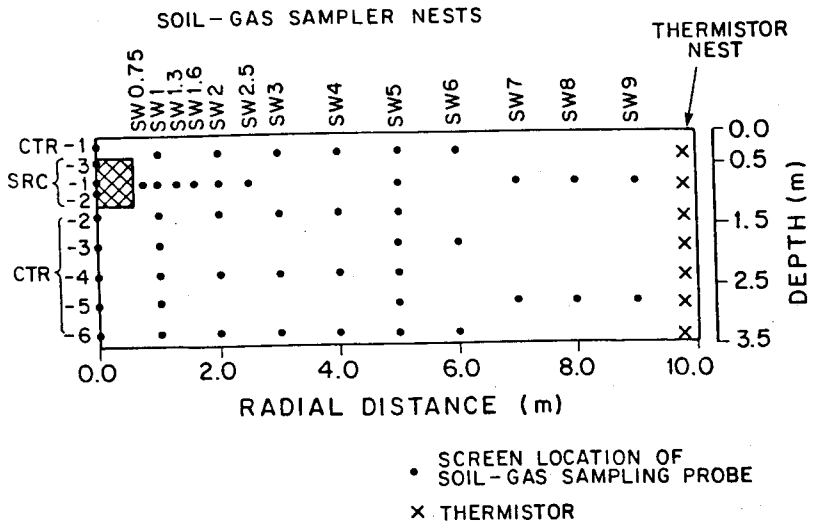

Figure 8. Location of instrumentation along the detailed (SW) sampling profile. Location of the source is indicated by the cross-hatched rectangle. Individual soil gas sampling points are referenced with the labeling system SW*a*-*b* where *a* is radial distance of sampling nest from source in meters, and *b* is sampler number in sequence from shallowest to deepest for each sampler nest.

Sampling and Analysis

In order to accurately measure large concentration gradients over short distances and to minimize physical disturbance of the vapor plume by sample extraction, small-volume samples of soil gas were collected from closely spaced locations within the unsaturated zone. All samples were analyzed on site using a portable gas chromatograph (GC). This permitted determination of "real-time" data, early detection of sample probe problems, and strategic adjustment of the monitoring schedule. A detailed discussion and evaluation of the sampling methodology is provided by *Hughes et al.* [1992].

Sixty-two soil gas sampling probes were installed at the site in multilevel nests (Figure 3). The probes were constructed of 3-mm ID stainless-steel tubing with a 1-cm-long intake screen. Installation of the probes was accomplished by driving them to the desired depth using a hand-held, clamp-and-hammer assembly. A Mininert™ valve was attached to the upper end of each probe. Forty-nine of the sampling probes were installed in nested locations along the detailed sampling profile (Figure 3); the depths of the individual screens and locations of each sampling nest along this profile are indicated in Figure 8. The remaining 13 probes were installed at seven locations along different radial axes to allow an evaluation of the symmetry of vapor migration (Figure 3).

Prior to collecting soil gas samples, a volume of soil gas equivalent to 3 to 4 times the internal volume was purged from each probe. Following purging, soil gas samples, ranging in volume from 5.0×10^{-5} L to 1×10^{-2} L, were collected using glass syringes. The soil gas probes were constructed with very small internal volumes (5×10^{-3} L to 3×10^{-2} L) to minimize any effects of the sampling procedure on vapor movement [*Hughes et al.*, 1992]. If a spherical zone of influence is assumed around each sampling point, the combined purging and sampling procedures correspond to radii of influence of only 0.02 to 0.04 m. Therefore sampling rounds involved removal of only a very small fraction of the total pore space occupied by the plume.

Soil gas samples were analyzed on site using a Photovac model 10S70 GC with a capillary column (CPSil5CB) and an isothermal column oven. Injections of all samples to the GC were performed manually using Gastight™ syringes. The GC was calibrated daily by direct injection of gas standards prepared on site from liquid stock solutions. Calibrations were performed in units of parts per million by volume (ppmv) and in a manner to account for subsurface temperature variations on sample concentrations [*Hughes et al.*, 1992].

Statistical analysis of the results to determine data precision for the combined sampling and analysis procedure indicates 95% confidence intervals on concentration values of approximately ±20% and ±10% for experiment 1 and experiment 2, respectively [*Hughes et al.*, 1992].

Results and Discussion

Experiment 1 (Winter, Covered)

Soil gas concentrations were monitored over a period of 26 days for experiment 1. Vapor concentrations along the detailed monitoring profile are presented in Figure 9 for 6 selected days. Concentration contours in these plots are expressed as the logarithm of TCE vapor concentration, with the outer contour (labeled −1) on each plot representing a TCE vapor concentration of 10^{-1} ppmv. In each case the bottom dashed line in the plot corresponds to the depth of the capillary fringe at the time of sampling. The unsaturated zone thickness remained relatively constant over the course of the experiment, with a total water table rise of 8 cm. Because the scale of monitoring in these experiments was insufficient to determine the vertical concentration gradient near the top of the capillary fringe, concentration contours are inferred near the base of the unsaturated zone. It is assumed that vapor diffusion in this region is slow because of the high soil moisture contents.

A maximum TCE vapor concentration of 22,000 ppmv was measured from probes within the TCE source zone, but source concentrations were more typically in the range of 10,000 to 16,000 ppmv for most of the experiment. These concentrations represent only 35 to 60% of the theoretical vapor pressures

(approximately 30,000–36,000 ppmv) for the prevailing subsurface temperatures. It is believed that condensation of vapors curred as samples were drawn slowly through the colder tion of the steel sampling tubes above ground surface. Atmospheric temperatures were consistently at least 2° to 5°C lower than temperatures at the source depths, and measured source concentrations are more consistent with theoretical vapor pressures (approximately 17,000–22,000 ppmv) for the atmospheric temperatures. As is discussed below, source concentrations measured during the summer (experiment 2) are more consistent with theoretical values.

The results from experiment 1 provide an indication of the speed with which a vapor plume can develop in a sandy, porous medium. Within only a few days, a vapor plume had migrated downward to the capillary fringe and traveled laterally several meters. The relatively even spacing of logarithmic contours reflects an exponential drop in vapor concentrations with distance from the source, and the rate of advance of the plume front decreases as the plume expands over time. Vapor migration rates were slower near the surface than at depth. This slower near-surface migration persists throughout experiment 1 and becomes more apparent with increasing distance from the source and increased travel time.

It is assumed that the surface cover in this experiment prevented significant loss of vapors from shallow sediments to the atmosphere. Among the possible factors contributing to the more rapid migration at depth are density-driven advection and greater near-surface retardation caused by the variable transport parameters and material properties. The potential influences of variations in temperature, moisture content, organic carbon content, and intrinsic permeability on transport re explored below.

The increase in temperature with depth in experiment 1 (Figure 6) corresponds to an increase in the diffusion coefficient and Henry's constant, favoring more rapid diffusion and decreased retardation with depth. This expectation is consistent with the observed concentration contours.

Spatial variations in moisture content are also consistent with the observed plume geometry. As seen in Figure 5b, the organic horizon, although thin, has a moisture content twice that of the underlying sediments. This layer and other higher moisture content zones in the upper section could have a diffusive "barrier" effect because the increased moisture contents greatly decrease diffusion coefficients in these zones. In addition to the barrier effect, these high moisture content zones act as contaminant vapor "sinks" retarding plume movement by dissolution of the TCE vapor in the soil moisture. A reduced potential for advective transport also exists in high moisture content zones due to decreased gas phase permeabilities. However, permeability variations are not believed to be important for experiment 1 because, as is discussed further below, transport was dominated by diffusion.

The large variations in organic carbon content at the site also favor much greater sorptive retardation in the upper sediments, consistent with the observed results. The contours in Figure 9 show a break in the slope of the contours near the organic horizon at the division between the upper and lower sections of sediments.

Thus the observed geometry of the vapor plume for experiment 1 is consistent with both greater retardation at shallow depths due to vapor dissolution and sorption, and an increase in diffusion rates with depth. Density advection, if significant, could also cause more rapid migration at depth. Although the experimental results are consistent with theoretical considerations, they can be explained by any combination of the aforementioned factors. The relative importance of each factor to transport cannot be directly determined on the basis of this single data set. A numerical sensitivity analysis, presented later, explores the relative importance of these factors for transport.

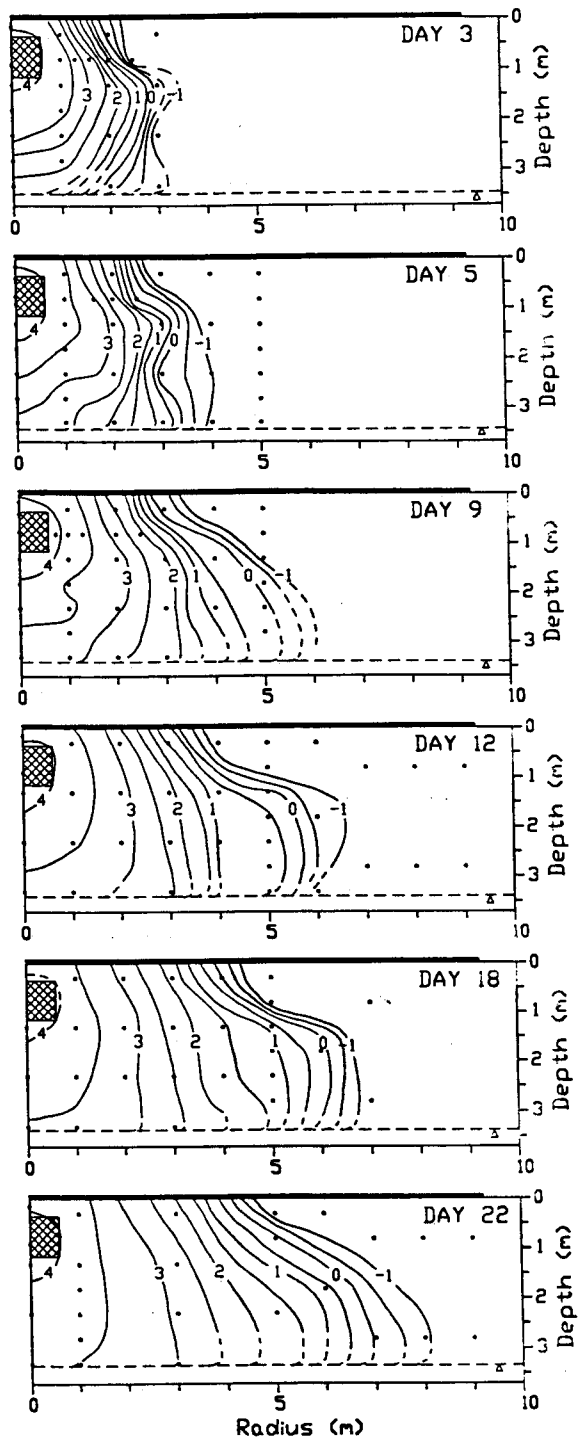

Figure 9. Contoured profiles of TCE vapor concentration from experiment 1 (winter) for six selected sampling events. Contours are in logarithm of vapor concentration in parts per million by volume (ppmv).

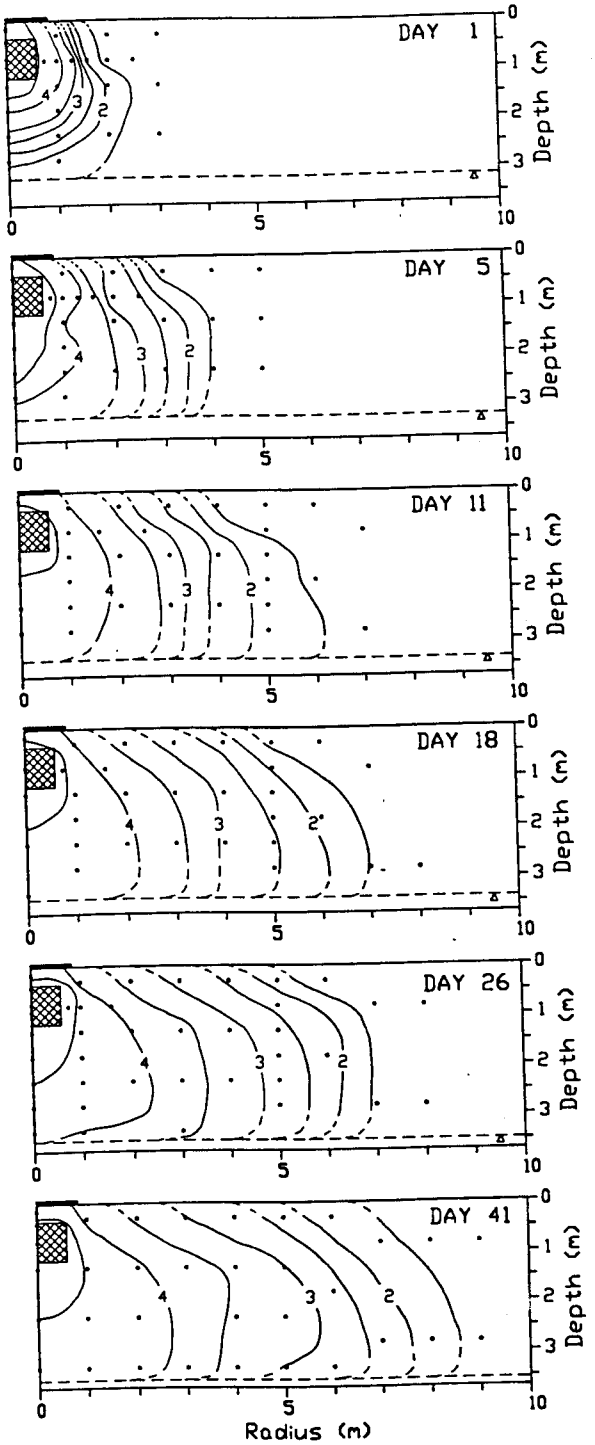

Figure 10. Contoured profiles of TCE vapor concentration from experiment 2 (summer) for six selected sampling events. Contours are in logarithm of vapor concentration in ppmv.

Experiment 2 (Summer, Uncovered)

Soil gas concentrations were monitored for a period of 41 days for experiment 2. Contours of TCE vapor concentration for six selected days are presented in Figure 10. The plots are configured similarly to Figure 9, except that the plume is contoured only to a concentration value of $10^{1.5}$ (32) ppmv because residual TCE vapor concentrations from experiment 1, of the order of 5 to 15 ppmv, made plume mapping unreliable at low concentrations. At very shallow depths the contours have been extrapolated to asymptotically approach the ground surface. This reflects the assumption that the ground surface represents a constant zero-concentration boundary. Reliable measurement of this near-surface vertical gradient would require additional sampling over much smaller depth increments. No measurements were attempted of air quality immediately above the ground surface.

No precipitation occurred for the first 20 days of experiment 2, and a total of 4.1 cm of rain fell between day 21 and day 41. Because the sediments were shown to be well drained immediately prior to the experiment, the moisture content in the unsaturated zone was believed to be constant for at least the first 20 days. For the purpose of the numerical simulations, moisture content was assumed constant for the entire experiment. The water table elevation declined continuously over the course of the experiment, with a total drop of 44 cm.

Vapor concentrations in the source area for experiment 2 were significantly higher than those measured in experiment 1. The maximum vapor concentration obtained from within the source was 88,000 ppmv, but concentrations were generally within the range of 55,000 to 75,000 ppmv. These concentrations compare more favorably with theoretical values than experiment 1; they represent approximately 75 to 98% of the theoretical vapor pressure values (73,500–90,000 ppmv) corresponding to the measured temperatures in the source area. Vapor condensation did not pose a problem for this experiment because atmospheric temperatures were warmer than temperatures at depth. As a result of the higher concentrations in the source region, the total contaminant mass contained in the vapor plume in experiment 2, for any given radial extent of plume migration, exceeded that of experiment 1.

The vapor plume spread more rapidly in experiment 2 than in experiment 1. A comparison of plume profiles for day 5 and day 18 for each experiment in Figures 9 and 10 demonstrates this faster spreading. However, the general characteristics of plume evolution in experiment 2 are similar to those for experiment 1. Concentrations declined exponentially with distance, rates of plume advance decreased with time, and retardation of the plume is evident in the upper meter or so of sediments.

The major differences in conditions between the two experiments are the nature of the surface boundary condition (covered versus uncovered) and the subsurface temperature profiles (winter versus summer). In the absence of other influences on transport, vapor loss at the ground surface in experiment 2 should result in a reduction in TCE vapor concentrations and a corresponding decrease in the plume migration rate relative to experiment 1. However, enhanced, rather than decreased, rates of transport were observed. This suggests that vapor transport was more strongly affected by the second factor, seasonal temperature change. An increase in subsurface temperatures causes higher vapor concentrations in the source area, resulting in a greater driving force for both diffusion and density-driven advection, an increase in the diffusion coefficient, and a decrease in retardation due to vapor dissolution and sorption. The more rapid spread of the plume downward, as opposed to laterally, in the immediate vicinity of the source (Figure 10) may indicate density effects. However, this preferential downward transport may also be due, in part, to inhibition of lateral diffusion by the presence of the organic layer.

Similar to experiment 1, the results for experiment 2 are consistent with shallow plume retardation due to higher or-

ganic carbon and moisture contents in the upper sediments. However, for experiment 2, the temperature trend with depth is opposite to that of experiment 1. The summer temperature profile favors decreasing diffusion rates and increasing retardation by vapor dissolution with depth, but these temperature-dependent effects are not discernible in the observed plume geometry. Thus the temporal (seasonal) increase in the overall temperatures in experiment 2, relative to experiment 1, was seen to have very significant effects on rates of transport, but spatial variations (depth trends) in temperature during the experiment are masked by other more dominant factors controlling plume geometry.

The relative contribution of increased sorptive retardation and vapor dissolution at shallow depths to the observed plume geometry cannot be unambiguously distinguished from possible density effects or the effects of losses of vapors to the atmosphere. However, an indication of the significance of spatial variations of physical properties in controlling vapor transport is provided by an examination of the degree of symmetry of transport observed in experiment 2.

To assess transport symmetry, TCE vapor concentrations along the detailed sampling profile were compared with sampling results along three other radial directions from the source (Figure 3). Figure 11 demonstrates the significance of geological changes across the site by a comparison of concentration trends for probes at each of the 5-m sampling nests. The shallowest samplers, at a depth of 0.3 m (Figure 11a), show a more rapid increase in concentrations for the samplers to the north of the source (NE5-1 and NW5-1) relative to those to the south (SW5-1 and SE5-1). This is consistent with the fact that the upper, organic-rich section of sediments thickens southward across the site. The difference in migration rates becomes less pronounced with depth below the organic horizon (Figure 11b), and migration is very symmetrical in the lower section where sediments are relatively uniform across the site (Figure 11c). Therefore radial symmetry of vapor transport from a uniform source appears likely in relatively homogeneous deposits, but as is illustrated for this site, transport may be significantly affected by directional heterogeneity of the geologic materials.

To expand the interpretation of results for both experiments and investigate further the relative importance for transport of various factors, including density advection, numerical modeling studies were performed. These studies included both simulation of the experimental results and additional sensitivity analyses.

Numerical Modeling Study

The numerical model used in this study is an axisymmetric, finite element model for vapor transport that incorporates density-induced advective gas flow as well as diffusive transport. The model is based on that described by *Mendoza and Frind* [1990a], modified to account for the effects of spatial temperature variations on transport parameters such as H and D_a [*Mendoza et al.*, 1992]. Previous numerical modeling studies of passive vapor transport of volatile organic compounds have used similar equations and theoretical assumptions but have generally been applied in simplified, homogeneous, and isothermal systems.

The experimental conditions were represented as realistically as possible by using either values measured at the site or the most appropriate literature values. The use of measured

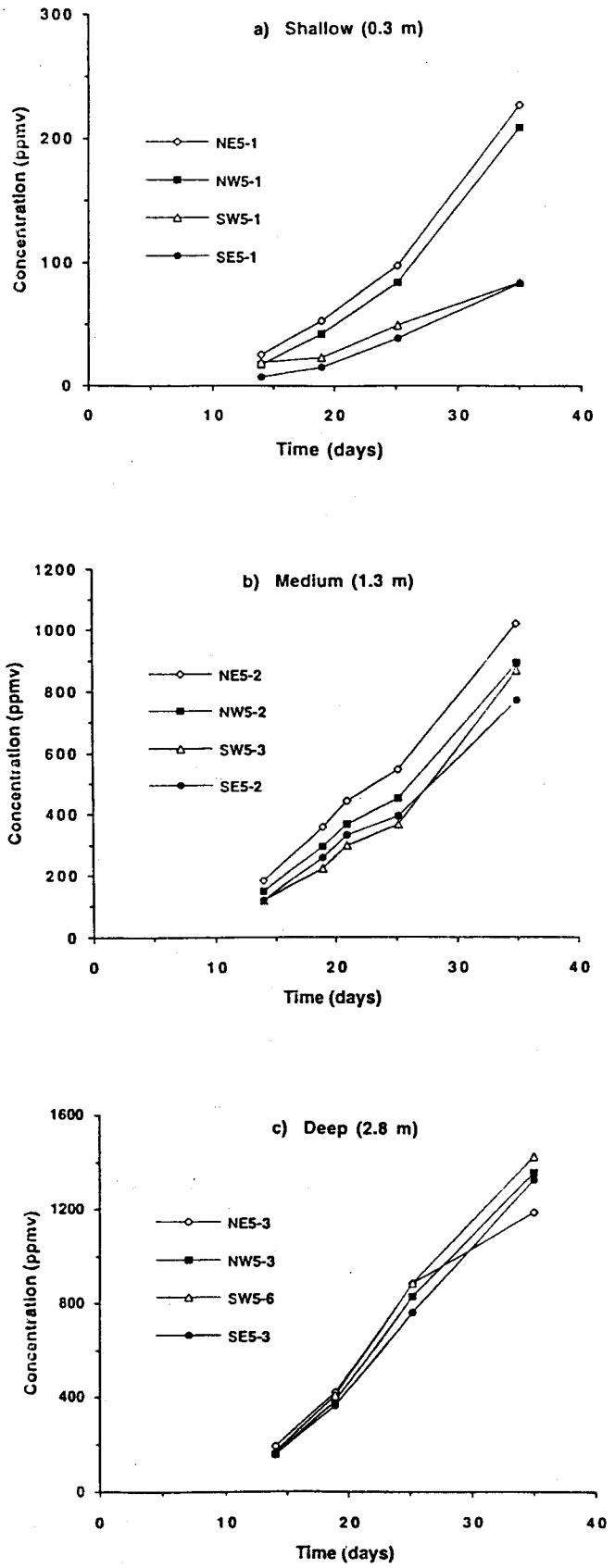

Figure 11. Vapor concentration versus time for experiment 2 for samplers from sampling nests at 5-m distance from the source. Concentrations are compared for each sampler nest at depths of (a) 0.3 m (shallow), (b) 1.3 m (medium), and (c) 2.8 m (deep).

Table 1. Input Parameters for Numerical Simulations

Parameter	Value
Porosity θ, %	40
Bulk density ρ_b, g cm^{-3}	1.48
Brooks-Corey pore size index λ	2.0
Longitudinal dispersivity α_L, m	0.5
Transverse dispersivity α_T, m	0.0
Organic partitioning coefficient K_{oc}, mL g^{-1}	126
Molecular weight of TCE, g mol^{-1}	131.4
Molecular weight of air, g mol^{-1}	28.75
TCE gas viscosity, Pa s	9.56×10^{-6}
Viscosity of uncontaminated soil gas, Pa s	18.0×10^{-6}

values in the numerical model allowed incorporation of macroscale variations in permeability, moisture content, and organic carbon content, and of the temperature dependence of diffusion coefficients, vapor density, and vapor-aqueous phase partitioning.

The results from experiment 1 were used as a base case for numerical simulation. The presence of a surface cover provided the most controlled conditions for a model comparison. Input parameters were based on field data or literature values. The only input parameter that was adjusted for the purpose of "fine tuning" the fit to the field data was longitudinal dispersivity. The very small impact that dispersion, and the advection process as a whole, has on the results for experiment 1 is further explored in the sensitivity analyses. Inclusion of a transverse dispersivity equal to one tenth of the longitudinal dispersivity made no observable difference to the simulation results.

The simulations were repeated for the experiment 2 conditions, with the model input from the base case simulations (experiment 1) modified only to reflect the open surface boundary, the appropriate changes in temperature-dependent parameters, and the presence of background vapor contamination from the first experiment. Following these simulations, several sensitivity analyses were performed to investigate further the relative contributions from advective flow, the surface boundary condition, and sorption.

Simulation Domain

Discretization of the finite element domain included vertical node spacings of 10 to 25 cm and horizontal spacings of 15 to 100 cm. Initial time steps of 1.0 to 2.4 hours were used to provide a combination of spatial and temporal discretizations satisfying Peclet and Courant stability and accuracy criteria [*Daus et al.*, 1985] to minimize any effects of numerical dispersion. Nodes coincided with the locations of the soil gas samplers along the detailed southwest sampling profile. Elements were configured within 20 laterally homogeneous layers to reflect the depth variation in permeability, organic carbon content, moisture content, and temperature. The lower boundary of the domain was set at 3.45 m, the average depth to the top of the capillary fringe.

All simulations were performed in an axisymmetric coordinate system with a vertical axis of rotation through the center of the cylindrical source zone. The left lateral boundary was represented by an impermeable symmetry boundary condition. Nodes corresponding to the location of the residual liquid source were assigned constrained vapor concentrations equivalent to the equilibrium vapor pressure for the temperature at that depth. Vapor pressures were calculated according to the relationship of *Stephenson and Malanowski* [1987]. The right lateral boundary for simulation of both experiments was set at 14 m from the source and was a constant pressure boundary with zero dispersive flux. The 14-m distance was established, on the basis of sensitivity analyses, as being sufficiently far from the source so as not to impact the transport solution (on plots presented in this paper, the domain has been truncated at 10 m for convenience). The lower boundary of the domain was treated as impermeable to both air flow and vapor transport.

For simulation of experiment 1 (covered), the upper boundary from 0 to 9 m from the source was treated as impermeable to air flow and vapor transport. In this case, effects of diffusion or any gas leakage through the cover were not considered; simulations using a "permeable" constant pressure and zero concentration upper boundary are considered in the sensitivity analysis. A constant pressure, zero concentration condition was assigned to the upper boundary from 9 to 14 m from the source, and an initial condition of zero concentration was assigned to all nodes outside of the source.

For experiment 2, the open ground surface from 0.8 to 14 m was represented by a zero-concentration boundary at constant atmospheric pressure. To represent the effects of residual vapor contamination, nodes outside the source were assigned an initial concentration of 10 ppmv in the upper 30 cm and 15 ppmv for the remainder of the domain.

Gas phase permeabilities were assigned to each layer on the basis of a single averaged profile of permeability measurements made at the site. Moisture contents and temperature varied with depth but were held constant in time. Henry's constants were calculated using the relationship of *Munz and Roberts* [1987], and diffusion coefficients were calculated according to *Green* [1984]. Table 1 summarizes the input parameter values for constants used in the simulations, while Figures 1, 2, 5, 6, and 7 illustrate the range of important space- and temperature-dependent parameters.

Comparison of Measured and Simulated Results

Under conditions of the test, the match obtained between the numerical simulations and the field data was very good for both experiments. An example of the quality of the match for the contoured concentration profiles is given for day 18 of each experiment in Figure 12. The field data were contoured by hand, whereas the simulation results were contoured over the entire finite element grid, and the sampler locations are shown for reference only on those plots.

Although the simulations predict the overall geometry and extent of the plume very well, they overpredict retardation of the shallow vapor plume for experiment 1 and the plume front at depth in experiment 2. The discrepancy between the simulations and field data may be due, in part, to an inadequate representation of heterogeneity in the shallow sediments. The vertical organic carbon profile used in the simulations was based on a single field core; however, the sediments were observed in the field to be both laterally and vertically heterogeneous, particularly in the upper meter. In experiment 1 the simulations predict higher concentrations near the source than were measured. The low field values are attributed to difficulties in measuring saturated vapor concentrations, as was discussed earlier. For the numerical simulations, use of the theoretical, temperature-dependent vapor concentrations was found to provide a much better overall match to the field data outside the source area.

The ability of the numerical model to predict the field behavior of vapor migration under two different sets of conditions suggests that it provides a reasonable representation of the physical processes governing vapor transport at the scale of measurement. It also suggests that many of the assumptions inherent in the theory used to describe that transport are appropriate for this setting. This provides increased confidence in the model as a tool to investigate the sensitivity of transport to major transport variables. Given this confidence, the model was used to calculate the mass of contaminant within the vapor plumes.

The total mass of TCE liquid used in the source zone in each experiment was approximately 60 kg. Table 2 summarizes the contaminant distribution within the plume (exclusive of the source) for day 18 of each experiment. The table shows that by day 18 of the experiment 1 and 2 simulations, approximately 11% and 24%, respectively, of the original TCE residual liquid had migrated away from the source by vapor transport.

The total mass of TCE contained within the vapor-contaminated zone was greater for experiment 2 as a result of greater distance of radial migration and the higher vapor concentrations in the vicinity of the source. In addition, 6.0 kg of TCE were estimated to have been lost at the surface boundary, an amount almost equivalent to the total mass of TCE contained within the zone of contamination for experiment 1. In both experiments the largest portion of the contaminant mass, outside of the source itself, is contained in the sorbed phase. This sorbed mass is less in the experiment 2 simulations than for experiment 1, despite the fact that the total mass in aqueous solution is larger. The much higher temperatures in experiment 2 in the shallow, more organic-rich sediments resulted in significantly increased partitioning to the vapor phase in these deposits, making less dissolved phase contaminant available for sorption.

Table 2. Numerical Simulation Mass-Fate Calculations, Day 18

	TCE Mass, kg	
	Experiment 1	Experiment 2
Vapor phase	0.6	1.8
Dissolved phase	1.2	2.3
Sorbed phase	5.2	4.6
Total mass*	7.0	8.7
Surface losses	negligible	6.0

*Excluding source zone.

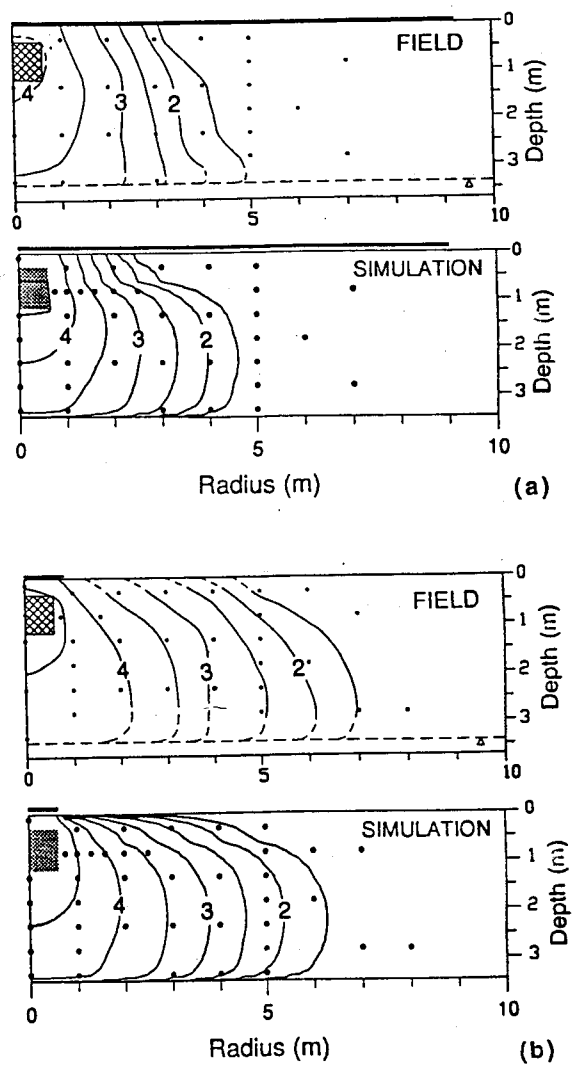

Figure 12. Comparison of field data and numerical simulations for day 18 of (a) experiment 1 and (b) experiment 2. Contours are in logarithm of TCE vapor concentration in ppmv.

Because of the short duration of the experiments, the effects of differential rates of mass loss and changing source distribution on source depletion were not considered. In addition, mass loss across the lower boundary of the domain by aqueous diffusion of dissolved vapors was not considered; however, it is expected to be negligible over the timescale of this study.

Sensitivity Analyses

Overall plume geometry in both field experiments was similar. However, because more than one variable changed between the two experiments, the comparison of field results cannot provide a unique interpretation of the controlling influences. Although the important influence of seasonal temperature variation on vapor transport is indicated by the field results, the magnitude of the effect of other processes on plume geometry is less clear. Therefore sensitivity analyses were performed to investigate the contribution of three different factors to plume evolution: density-induced advection, the surface boundary condition, and organic carbon content.

Since the density-induced advection of vapor is concentration dependent, it is most significant in the vicinity of the residual source liquid where vapor concentrations are highest. Downward advective gas velocities in the vicinity of the source, as calculated by the numerical model, were approximately 15 cm d^{-1} for experiment 1 and 50 cm d^{-1} for experiment 2. To investigate the significance of this advective component of transport to the overall plume migration, a comparison was made between simulation of each experiment, with and without advection.

Figure 13 shows comparisons between the full transport solution (dashed line) and the solution without advection (solid line) along the contoured profile for day 18 of the simulation for each experiment. The results indicate that advection causes increased plume migration in both cases but is less pronounced

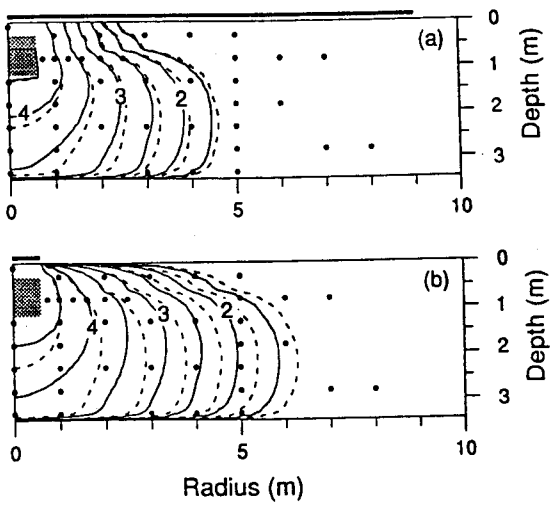

Figure 13. Comparison of simulations incorporating the full transport solution (dashed contours) to a numerical simulation ignoring advection (solid contour) for day 18 of (a) experiment 1 and (b) experiment 2. Contours are in logarithm of ppmv.

in experiment 1. The effect is greater in experiment 2 as a result of the higher concentrations and, consequently, higher vapor densities in the source area. For both experiments the effect is greater at depth than in the upper sediments.

To investigate the sensitivity of the transport process to the surface boundary condition, each experiment was simulated using the ground surface boundary condition for the other experiment; that is, the simulation for experiment 1 was repeated for an open surface boundary condition, except for a small cover directly over the source, and experiment 2 was simulated with an impermeable surface boundary. A comparison of the results of these "reversed cover" simulations (solid contours) to those for the original simulations (dashed contours) is shown in Figure 14 for day 18 of each experiment.

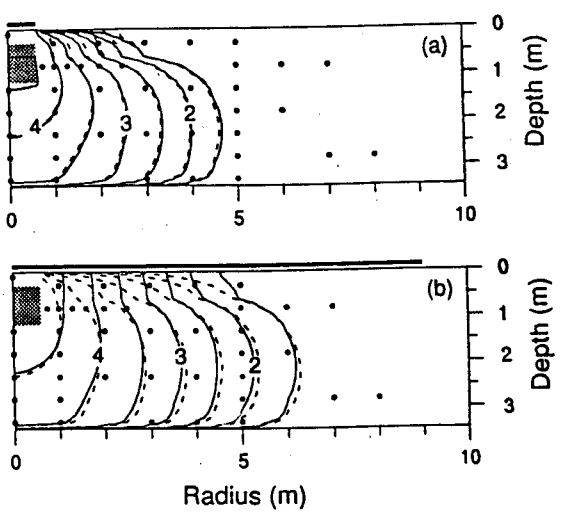

Figure 14. Comparison of simulations with varied surface boundary conditions for (a) experiment 1 and (b) experiment 2. Original simulation conditions (experiment 1, covered; experiment 2, uncovered) are represented by dashed contours. Solid contours represent the reverse conditions (experiment 1, uncovered; experiment 2, covered). Contours are in logarithm of ppmv.

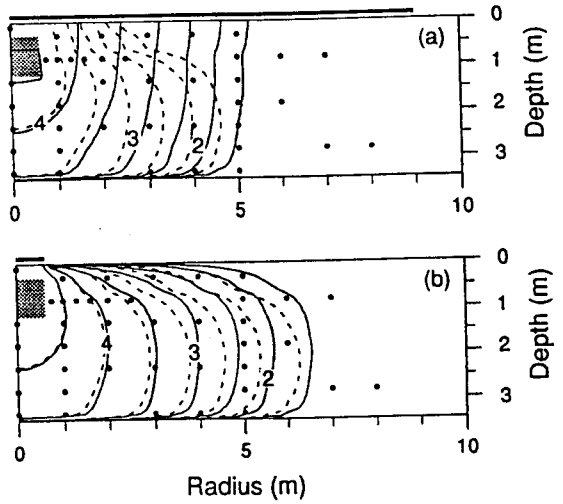

Figure 15. Comparison of simulations with varied organic carbon content for (a) experiment 1 and (b) experiment 2. Simulations using original, field-based, organic carbon distributions are represented by dashed contours. Solid contours reflect simulations using a uniform value of f_{oc} = 0.00014. Contours are in logarithm of ppmv.

Removal of the cover in experiment 1 (Figure 14a) has a negligible effect on the numerical simulation at depth. In the very shallow sediments it causes an increased retardation of the plume as a result of vapor loss to the atmosphere. Under winter conditions it appears that transport at this site is relatively insensitive to the surface boundary condition. The addition of a cover for experiment 2 (Figure 14b) results in slightly slower migration of the plume at depth and a more rapid migration rate in the shallow sediments relative to the uncovered case. The reduced migration at depth results from the reduced advective circulation of air through the source caused by the addition of a cover [*Mendoza and Frind*, 1990b]. The increased migration at shallow depth results from the reduction of vapor losses to the atmosphere.

The sensitivity of the transport process to the organic carbon content was investigated by comparing the initial simulations for each experiment to simulations in which the entire solution domain was assigned an f_{oc} value of 0.00014. This corresponds to the lowest f_{oc} value assigned to the sediments in the initial simulations. The results for day 18 of each experiment are presented in Figure 15. The simulation for experiment 1 (Figure 15a) indicates no retardation of vapor transport in the shallow sediments relative to the lower section and the entire plume migrates further radially. The slight retardation at the base of the plume reflects the slower vapor migration in the higher moisture content sediments near the capillary fringe. The influence of the thin, high moisture content layer at about 60-cm depth can be seen as a very small indentation in the contours. The simulation for experiment 2 (Figure 15b) also indicates more rapid vapor migration resulting from the decreased retardation in the upper section. However, the plume maintains a curvature of the contours at very shallow depth resulting from the loss of the vapors to the atmosphere at surface.

These simulations indicate that the distribution of organic carbon within the sediments at this site has a very strong influence on the relative migration rates of the TCE vapor in each experiment. The increased sorption of TCE to the higher

organic carbon sediments in the upper section acts as a contaminant sink and makes transport relatively insensitive to the nature of the surface boundary condition.

Conclusions

The Borden vapor transport experiments provide a detailed example of vapor migration from a source of liquid TCE in a shallow, sandy, unsaturated zone. Mapping of the soil gas contaminant plumes indicated that vapor transport of volatile chemicals can result in relatively rapid contaminant migration. In both field experiments a vapor plume migrated several meters laterally and downward to the capillary fringe within only a few days. Because vapor migration can contribute to the contamination of the underlying saturated zone, vapor transport is seen as a mechanism of rapid spread of volatile contaminants in the subsurface and a potentially important mechanism for groundwater contamination.

The observed transport behavior at the Borden field site was found to be consistent with theoretical predictions. A comparison of the results for winter and summer conditions showed that seasonal temperature variations can have a strong effect on source concentrations, rates of vapor transport, and mass of contaminant transported. Numerical sensitivity analyses indicated that diffusion generally dominated over advection but that advective effects were appreciable under the higher vapor concentration gradients encountered in the summer experiment. Variability in organic carbon content at the site was found to exert significant control over the relative rates of migration at different depths. Geometry of the vapor plumes observed for the field experiments was consistent with the expected influence of depth variation in organic carbon content and moisture content. Depth variation in temperature had a minor influence.

Observations of variable migration rates with radial direction from the source, numerical sensitivity analyses, and mass fate calculations suggest that the retardation at shallow depth in both experiments was primarily due to organic-rich sediments acting as a sorptive sink for TCE vapors. The presence of these shallow, organic-rich sediments made the experimental results relatively insensitive to the surface boundary condition. Significantly different results might be expected for a site characterized by only low-organic aquifer sands or glacial till. Variations in moisture content did not appear to have a strong influence on migration. However, it is anticipated that variations in moisture content could have a pronounced effect on vapor transport at other sites through its effect on gas phase permeability, the value of the effective diffusion coefficient, and the amount of retardation due to dissolution of vapors.

Simulations of the experiments using a finite element model for vapor transport provided a very good fit to the data when site-specific input parameters were used. The ability of the model to correctly represent the observed behavior for two different transport scenarios provided increased confidence in its applicability at this site. Comparison of the field experiments to numerical simulations was consistent with earlier numerical modeling studies suggesting that the sands of the Borden site are near the lower boundary of permeability for which advective flow would be significant for solvent vapor transport. The assumptions of equilibrium between contaminant phases, and sorption described by aqueous-solid partitioning proportional to organic carbon content, appear to be adequate to describe vapor transport at the Borden site. While sorption in the low organic content sands may be underpredicted by a correlation with organic carbon, it is likely that the net transport behavior in the lower sediments was not very sensitive to such a correlation.

The numerical simulations performed in this study incorporated spatial variations in transport parameters, and input parameters were based on detailed measurements conducted at the site. The results of these experiments reinforce the importance of incorporating the effects of heterogeneities of aquifer properties when interpreting contaminant distributions during site investigations. The degree of characterization necessary to provide adequate representation of spatial and temporal variability, at an appropriate scale of measurement, will be different for each site.

The Borden vapor transport experiments provide insight into the relative importance of various controls on organic vapor transport for a single geological setting. Also, these experiments evaluated transport over relatively short time periods as compared with the typically longer periods between releases and site investigations at most contaminated sites. The long-term effects on migration of infiltration and source depletion were not investigated, nor was the effect of source geometry. Additional field studies in a variety of geological environments are required to gain a better understanding of the kinds and magnitudes of parameter variations that are important for transport and remediation. The use of numerical sensitivity analyses is recommended both in the optimization of future field studies and in the interpretation of results.

Acknowledgments. The authors wish to thank the three anonymous reviewers who provided many helpful comments and suggestions for improvements to the manuscript. This research was conducted with funding from the University Consortium for Solvents-In-Groundwater Research supported, at the time of the research, by Ciba-Geigy, Dow Chemical, General Electric, and Eastman Kodak companies, and by the Natural Sciences and Engineering Research Council (NSERC) of Canada. Funding in the form of an NSERC postgraduate scholarship to B.H.C. is also gratefully acknowledged.

References

Abriola, L. M., C. Fen, and H. W. Reeves, Numerical simulation of unsteady organic vapor transport in porous media using the dusty gas model, in *Subsurface Contamination by Immiscible Fluids*, edited by K. U. Weyer, pp. 195–205, A. A. Balkema, Rotterdam, Brookfield, Vt., 1992.

Baehr, A. L., Selective transport of hydrocarbons in the unsaturated zone due to aqueous and vapor phase partitioning, *Water Resour. Res.*, *23*(10), 1926–1938, 1987.

Baehr, A. L., and C. J. Bruell, Application of the Stefan-Maxwell equations to determine limitations of Fick's law when modeling organic vapor transport in sand columns, *Water Resour. Res.*, *26*(6), 1155–1163, 1990.

Ball, W. P., C. H. Buehler, T. C. Harmon, D. M. Mackay, and P. V. Roberts, Characterization of a sandy aquifer material at the grain scale, *J. Contam. Hydrol.*, *5*(3), 253–295, 1990.

Bear, J., *Dynamics of Fluids in Porous Media*, Am. Elsevier, New York, 1972.

Bird, R. B., W. E. Stewart, and E. N. Lightfoot, *Transport Phenomena*, 780 pp., John Wiley, New York, 1960.

Boublik, T., V. Fried, and E. Hala, *The Vapor Pressure of Pure Substances*, 2nd rev. ed., Elsevier, New York, 1984.

Brooks, R. H., and A. T. Corey, Hydraulic properties of porous media, *Hydrol. Pap. 3*, 27 pp., Colo. State Univ., Fort Collins, 1964.

Chiou, C. T., and T. D. Shoup, Soil sorption of organic vapors and effects of humidity on sorptive mechanism and capacity, *Environ. Sci. Technol.*, *19*, 1196–1200, 1985.

Churcher, P. L., and R. D. Dickhout, Analysis of ancient sediments for

total organic carbon—Some new ideas, *J. Geochem. Explor.*, *29*, 235–246, 1987.

Cohen, Y., and P. Ryan, Multimedia modeling of environmental transport: Trichloroethylene test case, *Environ. Sci. Technol.*, *19*, 412–417, 1985.

Curtis, G. P., M. Reinhard, and P. V. Roberts, A natural gradient experiment on solute transport in a sand aquifer, 4, Sorption of organic solutes and its influence on mobility, *Water Resour. Res.*, *22*(13), 2059–2067, 1986.

Daus, A. D., E. O. Frind, and E. A. Sudicky, Comparitive error analysis in finite-element formulations of the advection-dispersion equation, *Adv. Water Resour.*, *8*, 86–95, 1985.

Dean, J. A. (Ed.), *Lange's Handbook of Chemistry*, 13th ed., McGraw-Hill, New York, 1985.

Dilling, W. L., Interphase transfer processes, II, Evaporation rates of chloromethanes, ethanes, ethylenes, propanes, and propylenes from dilute aqueous solutions: Comparisons with theoretical predictions, *Environ. Sci. Technol.*, *11*, 405–409, 1977.

Dilling, W. L., N. B. Tefertiller, and G. J. Kellos, Evaporation rates and reactivities of methylene chloride, chloroform, 1,1,1-trichloroethane, trichloroethylene and other chlorinated compounds in dilute aqueous solutions, *Environ. Sci. Technol.*, *9*(9), 833–838, 1975.

Falta, R. W., I. Javandel, K. Pruess, and P. A. Witherspoon, Density-driven flow of gas in the unsaturated zone due to the evaporation of volatile organic compounds, *Water Resour. Res.*, *25*(10), 2159–2169, 1989.

Flick, E. A. (Ed.), *Industrial Solvents Handbook*, 3rd ed., Noyes Data Corp., Park Ridge, N. J., 1985.

Freeze, R. A., and J. A. Cherry, *Groundwater*, 604 pp., Prentice-Hall, Englewood Cliffs, N. J., 1979.

Garbarini, D. R., and L. W. Lion, Evaluation of sorptive partitioning of nonionic pollutants in closed systems by headspace analysis, *Environ. Sci. Technol.*, *19*, 1122–1138, 1985.

Gossett, J. M., Measurement of Henry's law constants for C_1 and C_2 chlorinated hydrocarbons, *Environ. Sci. Technol.*, *21*, 202–208, 1987.

Green, D. W., *Perry's Chemical Engineer's Handbook*, 6th ed., McGraw-Hill, New York, 1984.

Hansch, C., and A. Leo, *Substituent Constants for Correlation Analysis in Chemistry and Biology*, John Wiley, New York, 1979.

Hughes, B. M., R. D. McClellan, and R. W. Gillham. Application of soil-gas sampling technology to studies of trichloroethylene vapor transport in the unsaturated zone, in *Ground-Water Contamination and Analysis at Hazardous Waste Sites*, edited by S. Lesage and R. E. Jackson, pp. 121–146, Marcel-Dekker, New York, 1992.

Hutzler, N. E., B. E. Murphy, and J. S. Gierke, Review of soil vapor extraction system technology, paper presented at Soil Vapor Extraction System Technology for Underground Storage Tank Sites Workshop, Risk Reduction Eng. Lab., U.S. Environ. Prot. Agency, Edison, N. J., June 27–28, 1989.

Karickhoff, S. W., Organic pollutant sorption in aquatic systems, *J. Hydraul. Eng.*, *110*(6), 707–735, 1984.

Larsen, T., P. Kjeldsen, T. H. Christensen, B. Skov, and M. Refstrup, Sorption of specific organics in low concentrations on aquifer materials of low organic carbon content: Laboratory experiments, in *Contaminant Transport in Groundwater*, edited by H. E. Kobus and W. Kinzelbach, pp. 133–140, A. A. Balkema, Rotterdam Netherlands, 1989.

Love, O. T., and R. G. Eilers, Treatment of drinking water containing trichloroethylene and related industrial solvents, *J. Am. Water Works Assoc.*, *74*, 413–425, 1982.

Mackay, D., and W. Y. Shiu, Critical review of Henry's law constants for chemicals of environmental interest, *J. Phys. Chem. Ref. Data*, *10*(4), 1175–1199, 1981.

Mackay, D. M., D. L. Freyberg, and P. V. Roberts. A natural gradient experiment on solute transport in a sand aquifer, 1, Approach and overview of plume movement, *Water Resour. Res.*, *22*(13), 2017–2029, 1986.

Massmann, J. W., Applying groundwater flow models in vapor extraction system design, *J. Environ. Eng.*, *115*(1), 129–149, 1989.

Massmann, J., and D. F. Farrier, Effects of atmospheric pressures on gas transport in the vadose zone, *Water Resour. Res.*, *28*(3), 777–791, 1992.

McWhorter, D. B., Unsteady radial flow of gas in the vadose zone. *J. Contam. Hydrol.*, *5*(3), 297–314, 1990.

Mendoza, C. A., and E. O. Frind, Advective-dispersive transport of dense organic vapors in the unsaturated zone, 1, Model development, *Water Resour. Res.*, *26*(3), 379–387, 1990a.

Mendoza, C. A., and E. O. Frind, Advective-dispersive transport of dense organic vapors in the unsaturated zone, 2, Sensitivity analysis, *Water Resour. Res.*, *26*(3), 388–398, 1990b.

Mendoza, C. A., and T. A. McAlary, Modeling of ground-water contamination by organic solvent vapors, *Ground Water*, *28*(2), 199–206, 1990.

Mendoza, C. A., B. M. Hughes, and E. O. Frind, Transport of trichloroethylene vapors in the unsaturated zone: Numerical analysis of a field experiment, in *Subsurface Contamination by Immiscible Fluids*, edited by K. U. Weyer, pp. 221–226, A. A. Balkema, Brookfield, Vt., 1992.

Millington, R. J., and J. P. Quirk, Permeability of porous solids, *Trans. Faraday Soc.*, *57*, 1200–1207, 1961.

Munz, C., and P. V. Roberts, Air-water phase equilibria of volatile organic solutes, *J. Am. Water Works Assoc.*, *79*(5), 62–69, 1987.

Peterson, M. S., L. W. Lion, and C. A. Shoemaker, Influence of vapor-phase sorption and diffusion on the fate of trichloroethylene in an unsaturated aquifer system, *Environ. Sci. Technol.*, *22*, 571–578, 1988.

Piwoni, M. D., and P. Banerjee, Sorption of volatile organic solvents from aqueous solution onto subsurface solids, *J. Contam. Hydrol.*, *4*, 163–179, 1989.

Poe, S. H., K. T. Valsaraj, L. J. Thibodeaux, and C. Springer, Equilibrium vapor phase adsorption of volatile organic chemicals on dry soils, *J. Hazard. Mater.*, *19*, 17–32, 1988.

Schwartzenbach, R. P., and J. Westall, Transport of nonpolar organic compounds from surface water to groundwater. Laboratory sorption studies, *Environ. Sci. Technol.*, *15*, 1360–1367, 1981.

Schwille, F., Migration of organic fluids immiscible with water in the unsaturated zone, in *Pollutants in Porous Media*, edited by B. Yaron, G. Dagan, and J. Goldshmid, pp. 27–48, Springer-Verlag, New York, 1984.

Schwille, F., *Dense Chlorinated Solvents in Porous and Fractured Media—Model Experiments*, translated from German by J. F. Pankow, Lewis, Boca Raton, Fla., 1988.

Sleep, B., and J. F. Sykes, Modeling the transport of volatile organics in variably saturated porous media, *Water Resour. Res.*, *25*(1), 81–92, 1989.

Smith, J. A., C. A. Chiou, J. A. Kammer, and D. E. Kile, Effect of soil moisture on the sorption of trichloroethylene vapor to vadose-zone soil at Picatinny Arsenal, New Jersey, *Environ. Sci. Technol.*, *24*, 676–683, 1990.

Stephenson, R. M., and S. Malanowski, *Handbook of the Thermodynamics of Organic Compounds*, Elsevier, New York, 1987.

Sudicky, E. A., A natural gradient experiment on solute transport in a sand aquifer: Spatial variability of hydraulic conductivity and its role in the dispersion process, *Water Resour. Res.*, *22*(13), 2069–2082, 1986.

Thomson, G. M., and D. L. Marrin, Soil gas contaminant investigations: A dynamic approach, *Ground Water Monit. Rev.*, *7*(3), 88–93, 1987.

Thorstenson, D. C., and D. W. Pollock, Gas transport in unsaturated zones: Multicomponent systems and the adequacy of Fick's laws, *Water Resour. Res.*, *25*(3), 477–507, 1989.

Weast, R. C. (Ed.), *CRC Handbook of Chemistry and Physics*, 68th edition, CRC Press, Boca Raton, Fla., 1987.

Weeks, E. P., D. E. Earp, and G. M. Thompson, Use of atmospheric fluorocarbons F-11 and F-12 to determine the diffusion parameters of the unsaturated zone in the Southern High Plains of Texas, *Water Resour. Res.*, *18*(5), 1365–1378, 1982.

B. H. Conant, 636 Red Pine Drive, Waterloo, Ontario N2V 1S1, Canada.

R. W. Gillham, Waterloo Centre for Groundwater Research, University of Waterloo, Waterloo, Ontario N2L 3G1, Canada.

C. A. Mendoza, Department of Earth and Atmospheric Sciences, University of Alberta, Edmonton, Alberta, T6G 2E3 Canada.

(Received November 7, 1994; revised September 14, 1995; accepted September 22, 1995.)